PAPER • OPEN ACCESS

Multi-objective optimization of sandwich composite pressure hull for decreasing weight and drag force and increasing buckling load capacity

To cite this article: Mahmoud Helal and Elsayed Fathallah 2020 *IOP Conf. Ser.: Mater. Sci. Eng.* **974** 012009

View the article online for updates and enhancements.

Military Technical College

Kobry El-Kobbah,

Cairo, Egypt

13th International

Conference on Civil and

Architecture Engineering

ICCAE-13-2020

Multi-objective optimization of sandwich composite pressure hull for decreasing weight and drag force and increasing buckling load capacity

Mahmoud Helal[1,2] and Elsayed Fathallah[3,4*]

[1]Department of Mechanical Engineering, Faculty of Engineering, Taif University, Taif 21974, Saudi Arabia

[2]Production and Mechanical Design Dept., Faculty of Engineering, Mansoura University, Mansoura 35516, Egypt

[3]Department of Civil Engineering, Military Technical College, Cairo, Egypt

[4]Ships and Submarines Engineering Department, Military Technical College, Cairo, Egypt.

* saidhabib2000@mtc.edu.eg & saidhabib2000@hotmail.com

Abstract:

In underwater applications, space vehicles, and aircrafts, the weight becomes an important factor. Additionally, the design of composites structures greatly depends on the number of layers and the fiber orientation angle. Therefore, this work presents the optimization of sandwich composite pressure hull in order to minimize (weight and drag force) and maximize the buckling load capacity using ANSYS Parametric Design Language (APDL). Tsai-Wu and maximum stress failure criteria were incorporated for predicting the first-ply failure. The major and minor radius of the pressure hull, the ring and long beams dimensions, the fiber orientation angle and layer thickness are taken as design variables. The results illustrated that, core thickness (T_{core}) has a great effect to resist the shell buckling. While, has a little effect on both Tsai-Wu and maximum stress failure index.

Keywords: Multi-objective optimization; Buckling; drag force; pressure hull; Tsai-Wu.

1. Introduction

The pressure hulls are one of the most main structures of the submarine which provide high load capacity for electronic systems and buoyancy [1]. The optimization and buckling behavior have been attracted some recent attention [1-17]. Additionally, Zhang et al. [18], investigated the egg-shaped pressure hulls to improve the low buckling resistance, the difficult interior arrangement and the poor hydrodynamics of the spherical pressure hull. Vosoughi et al. [19], investigated the optimum stacking sequences of laminated composite plate to maximize the buckling load by achieving the optimum fibers orientations. Significant research work had been presented so far in this field. Among them, Mian et al. [20], presented the design optimization procedure for a composite pressure vessel, considering both maximum stress and Tsai-Wu failure criteria. Pan et al. [21], studied the optimization of composite cylinder due to hydrostatic pressure. The ply orientation and thickness are studied. Furthermore, Fathallah and Helal [22], optimized deep cross elliptical pressure hull taking into consideration both buckling and failure criteria. Imran et al. [23], optimized a composite pressure hull to minimize the buoyancy factor. Lund [24], Optimized a laminated composite structures using failure criteria. Moreover, Fathallah et al. [25], investigated the optimization of elliptical composite pressure hull for minimizing buoyancy factor. In this wok, a sandwich composite pressure hull is proposed. The view of the model is shown in **Fig. 1**. The multi-objective optimization methodology for the pressure hull is presented. The optimization is established for maximizing the buckling load capacity and minimizing the drag force and (weight/displacement) ratio, of the pressure hull.
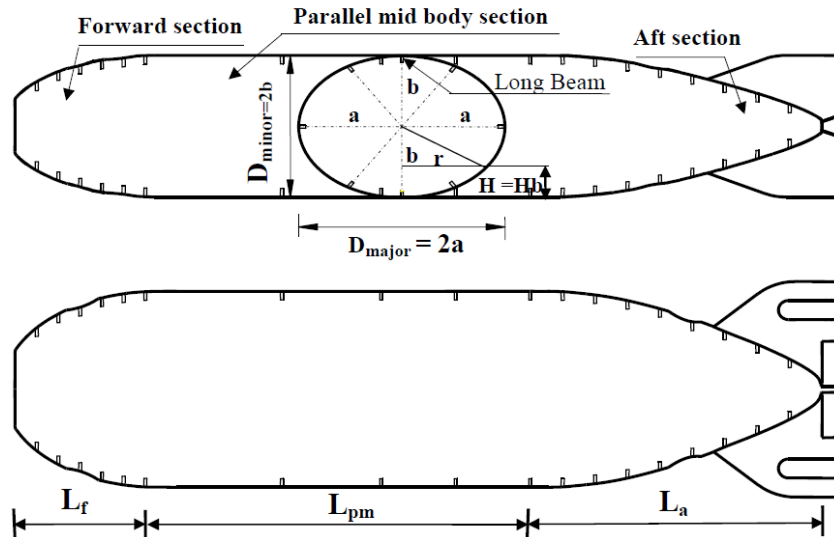
Fig. 1 Parameterization of the submersible pressure hulls geometry.

1.1 Buckling in multilayer-sandwich composite pressure hull

In this work, a scalar multiple λ of the design load, the so-called buckling load strength factor, is introduced to identify pre-buckling of the multilayer sandwich submersible pressure hulls and defined as [1]:

$$\lambda = \frac{P_S}{P_{act}} \tag{1}$$

Where: P_{act} is the actual load and P_s is the structural critical buckling strength. The buckling will occur when $\lambda < 1$ and (P_s) less than (P_{act}). The critical value of the pressure P_{cr} that will cause buckling is determined using the following equations [22, 26]:

$$P_{cr} = \left(\frac{R}{\left(n^2 + 0.5\left(\frac{m\pi R}{L} \right)^2 \right)} \right) \frac{\begin{bmatrix} C_{11} & C_{12} & C_{13} \\ C_{21} & C_{22} & C_{23} \\ C_{31} & C_{32} & C_{33} \end{bmatrix}}{\begin{bmatrix} C_{11} & C_{12} \\ C_{21} & C_{22} \end{bmatrix}} \tag{2}$$

Where: L, R, m and n are the length, the radius, the number of buckle half waves in the axial direction and the number of buckle waves in the circumferential direction, respectively. The coefficients C, A, B and D are defined as follows:

$$C_{11} = A_{11}\left(\frac{m\pi}{L}\right)^2 + A_{66}\left(\frac{n}{R}\right)^2, C_{22} = A_{22}\left(\frac{n}{R}\right)^2 + A_{66}\left(\frac{m\pi}{L}\right)^2$$

$$C_{33} = D_{11}\left(\frac{m\pi}{L}\right)^4 + (4D_{66} + 2D_{12})\left(\frac{m\pi}{L}\right)^2\left(\frac{n}{R}\right)^2 + D_{22}\left(\frac{n}{R}\right)^4$$

$$+\frac{A_{22}}{R^2} + 2\frac{B_{22}}{R^2}\left(\frac{n}{R}\right)^2 + 2\frac{B_{12}}{R^2}\left(\frac{m\pi}{L}\right)^2, C_{12} = C_{21} = \left(A_{12} + A_{66}\right)\left(\frac{m\pi}{L}\right)\left(\frac{n}{R}\right) \qquad (3)$$

$$C_{23} = C_{32} = \left(B_{12} + 2B_{66}\right)\left(\frac{m\pi}{L}\right)^2\left(\frac{n}{R}\right) + \frac{A_{22}}{R}\left(\frac{n}{R}\right) + B_{22}\left(\frac{n}{R}\right)^3$$

$$C_{13} = C_{31} = \frac{A_{12}}{R}\left(\frac{m\pi}{L}\right) + B_{11}\left(\frac{m\pi}{L}\right)^3 + \left(B_{12} + 2B_{66}\right)\left(\frac{m\pi}{L}\right)\left(\frac{n}{R}\right)^2$$

Where: A_{ij}, B_{ij} and D_{ij} are the stiffness components including extensional stiffness, coupling stiffness and bending stiffness coefficient matrix, respectively. The elements of the stiffness matrices are:

$$A_{ij} = \sum_{k=1}^{n} (\bar{Q}_{ij})_k (Z_k - Z_{k-1}), B_{ij} = \frac{1}{2}\sum_{k=1}^{n} (\bar{Q}_{ij})_k (Z^2_k - Z^2_{k-1}), D_{ij} = \frac{1}{3}\sum_{k=1}^{n} (\bar{Q}_{ij})_k (Z^3_k - Z^3_{k-1}) \quad (4)$$

Where: n is the number of different plies in the stacking sequence and Z_k, Z_{k-1} are the upper and lower (Z) coordinate of the k_{th} ply layer as shown in Fig. 2. $\bar{Q}_{ij}$ are the elements of the transformed reduced stiffness matrix $[\bar{Q}]$ and are defined as in [27]: The optimization can be achieved to obtain the highest buckling strength factor. The number of plies can be varied as well as their orientation. Since the fiber orientation has no influence on the mass function.
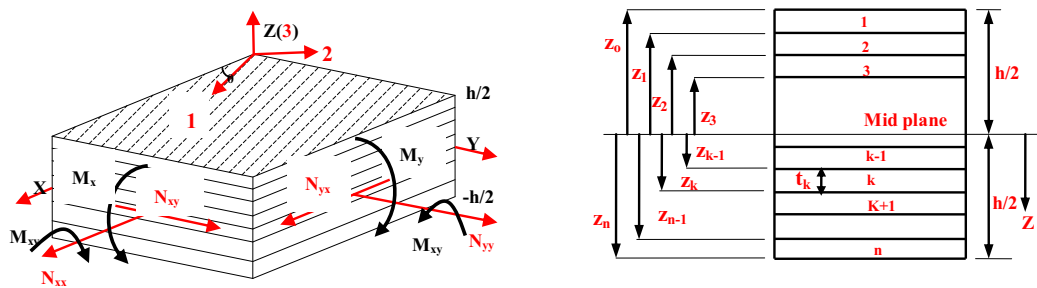
a)   A composite laminate subjected to forces and moments.   b)   Enlarged view of laminate cross-section

Fig. 2 Laminated composite shell and coordinate locations of plies in a laminate.

The successful design requires an efficient and safe use of materials. Therefore, theories are needed to develop and compare the state of the stresses and the strains in the material [28]. In

this study both Tsai-Wu and maximum stress failure criteria were incorporated for predicting the first-ply failure. and are defined as in [1]. The von Mises yielding criteria is employed here to assess the capability of the core materials to withstand the yielding failure.

1.2 Drag Estimation and power requirements

The proper hydro-dynamic design is necessary to achieve the effective performance of the submarine. An improper shape can cause excessive noise, drag and instability. Drag is the hydro-dynamic force exerted on the hull body in a direction opposite to its velocity. The propulsive power requirement is proportional to the drag and times the velocity divided by the propulsive efficiency. The drag is consist of two components, the form drag (function of the shape and frontal area) and friction drag (function of the speed and wetted surface area) [29]. For drag estimation, the following formula has been used [30]:

$$D = \frac{1}{2}\rho V^2 C_V S \tag{5}$$

Where: D denote the submarine drag in Newton (N), ρ denote the density of the fluid in kg/m^3, V denote the velocity in m/s, S denote the wetted surface area of the vehicle in m^2 and C_V denote the coefficient of viscous resistance for the smooth hull. There are three methods used to compute the coefficient of viscous resistance (C_V) namely; Virginia Tech, MIT and G&J method [31]. According to G&J method, the coefficient of the viscous resistance, C_V, can be calculated as [32]:

$$C_V = C_F \left[1 + 0.5\left(\frac{d}{L}\right) + 3\left(\frac{d}{L}\right)^3 \right] \tag{6}$$

In MIT method, C_V defined as:

$$C_V = C_F \left[1 + 1.5\left(\frac{d}{L}\right)^{\frac{3}{2}} + 7\left(\frac{d}{L}\right)^3 + 0.002(C_P - 0.6) \right] \tag{7}$$

Where: d denote the maximum body diameter in meters, L denote the total length in meters, C_F denote the bare hull skin friction drag coefficient and defined as a function of Reynolds number (R_n) as [33]:

$$C_F = \frac{0.075}{(\log_{10} R_n - 2)^2} \tag{8}$$

Where: C_P denote the prismatic coefficient and can be defined as:

$$C_P = \frac{V_d}{\pi \left(\dfrac{d}{2}\right)^2 L} \tag{9}$$

Where: V_d denote the displacement volume of the submarine in m^3, R_n denote the Reynolds number and can be defined as:

$$R_n = \frac{\rho V L}{\mu} \tag{10}$$

Where: ρ is the density of the fluid in kg/m^3, V is the velocity in m/s, L is the overall length of the submarine pressure hull in meters and µ is the dynamic viscosity of the fluid in kg/ (m.s). In this study, (V_d, S) will be calculated using volume and surface measurement function in ANSYS.

2. Submarines pressure hulls materials and simulation

The model constructed from Boron/Epoxy B(4)/5505 composites with the lay-up composed of sixteen plies (n = 16) having equal thicknesses (t_1) and fiber orientation angle (α) and one core layer with thickness (T_{core}). Low density PVC foam is used for the core layer. The material properties and strength parameters of B(4)/5505 Boron/Epoxy and PVC foam are given in **Table 1** [25, 34, 35]. **Fig.3** illustrates the relationship between the collapse depth and buoyancy factor for a visual comparison of different structural materials. [36]. The sandwich structure is modeled using Shell 281 element. The Beam 189 element is used for ring and long beams [37, 38].

Table 1. Strengths of unidirectional composites and material properties of the sandwich components [34, 35, 39, 40].

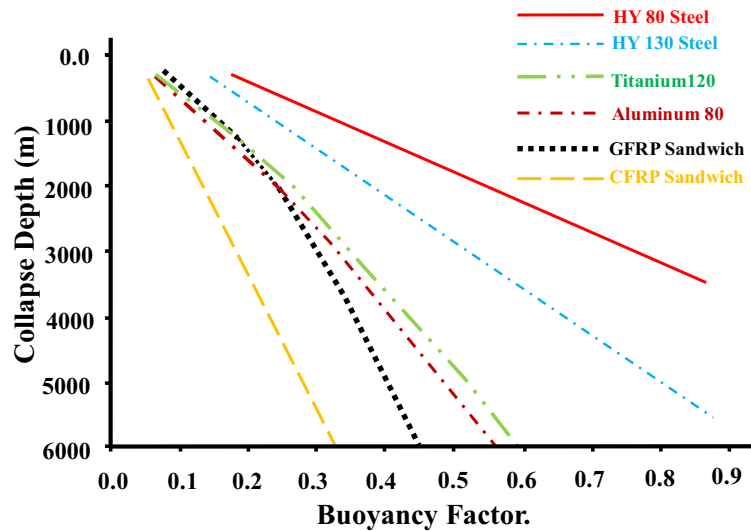| Material	Material and strength properties
B(4)/5505 Boron/Epoxy	E_{11}= 204GPa, E_{22}= 18.5GPa, , E_{33}= 18.5GPa, G_{12}= 5.59GPa, G_{13}= 5.59GPa, v_{12}=0.23, X_t=1260MPa, X_c=2500Mpa, Y_t=61MPa, Y_c=202MPa, S=67 MPa, ρ= 2000 kg/m^3
H200	E=250MPa, G=73MPa,v=0.3, X_t=7.1MPa, X_c=5.4Mpa, Y_t=7.1MPa, Y_c=5.4MPa, S=3.5MPa, ρ= 200 kg/m^3

Fig.3 Weight to displacement ratio Vs Collapse depth for stiffened cylinders.

The boundary conditions applied here as in [1, 41]. The pressure hull is loaded by external

pressure ($P = \rho gh$). Where ρ denotes the density of the sea water, g is the acceleration due to

the gravity and *h,* represents the operating depth. Two failure criteria, Tsai-Wu and maximum

stress are used to evaluate the failure of the pressure hull [25]. **Fig. 4**   shows the final layer

stacking for the global model.
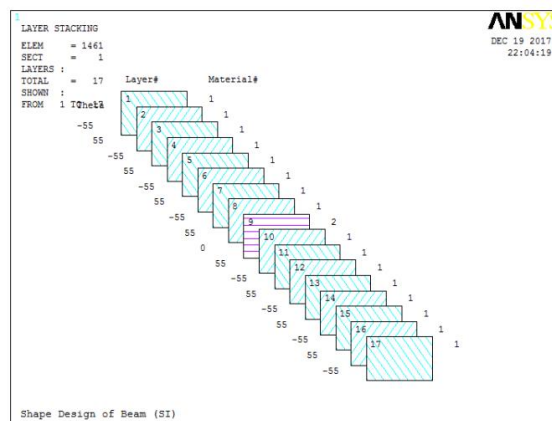
a)   Layer stacking

Fig. 4 The composite pressure hull layer stacking.

3. Structural design optimization

Fig.5 shows the flow chart of the multi-objective optimization procedure. The optimization

design is described as:

Objective function: F(X): Minimize (weight/displacement ratio (B.F) and drag force (D_F)) and maximize (buckling capacity (λ)).

Design constraints:

$$FS(i) \geq 1, \quad i = 1, 2, 3, \ldots n \tag{11}$$

Where: FS represents the factor of safety and must be greater than one to avert the first-ply failure of the angle-ply laminated for each ith layer and equals to the inverse of the failure index for both Tsai-Wu and maximum stress failure criteria and (n) is the number of layers.

$$\frac{\sigma}{\sigma_y} - 1 \leq 0 \tag{12}$$

Where: σ and σ_y are the actual stress and yielding strength in the core layer, respectively.

$$H \leq H_{\max} \tag{13}$$

Where: H, and H_{max} represent the operating depth and the maximum operating depth, respectively.

Design variables:

The composite pressure hull diameters are taken as:

$$D_i^L \leq D_i \leq D_i^U, i = \min, \max \tag{14}$$

Where: D_i, D_i^L and D_i^U are the ith submersible pressure hull diameters and its upper and lower limits, respectively.
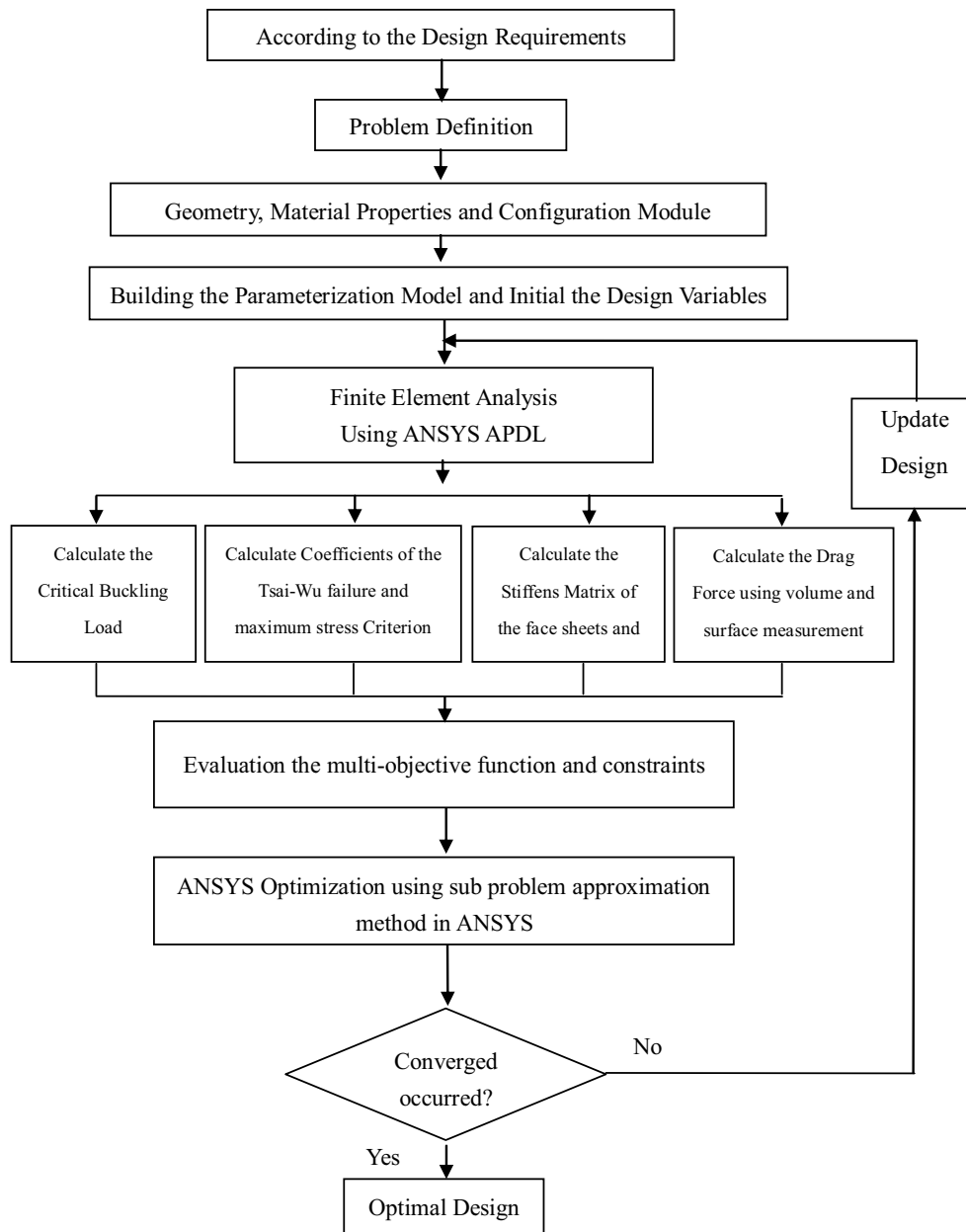
Fig.5 Flow chart layout of multi-objective optimization procedures

.

For core thickness:

$$T^{L} \leq T_{core} \leq T^{U} \tag{15}$$

Where: T_{core}, T^{L} and T^{U} represent the core thickness of pressure hull, and its lower and upper

limits, respectively. For ply thicknesses:

$$t^L \leq t_i \leq t^U, \ i = 1, 2, 3, ..., n \tag{16}$$

Where: t_i, t^L, t^U represent the ith thickness for the lower and upper bounds of the individual ply thicknesses, respectively.

$$\alpha^L \leq \alpha_i \leq \alpha^U, \quad i = 1, 2, 3, ..., n \tag{17}$$

Where: α_i, α^L, α^U represent the ith orientation angle of each layer and their lower and upper limits, respectively.

4. Results and discussions

The results of Multi-objective optimization are summarized in **Table 1**. The drag force is equals to 2.19925×10^{12} N, buckling strength factor (λ) equals 118, at ($B.F$) equals 0.47. The maximum magnitude of deflection value (δ_{max}) equal to 2.18 mm. **Fig. 6** illustrates the displacement distribution in X, Y and Z directions for the model. The maximum displacement occurs at the centroids regions of the composite pressure hull and occurs in vertical direction with value equals to 2.14 mm. The optimum configuration of the sandwich composite pressure hull can overcome all structural failures until operating depth (H) equals to 255 m.

Table 2. Results of the optimal design of the sandwich composite deep pressure hull.

FS_{TWSR_1}	FS_{TWSR_2}	FS_{TWSR_3}	FS_{TWSR_4}	FS_{TWSR_5}	FS_{TWSR_6}	FS_{TWSR_7}	FS_{TWSR_8}
1.59	1.63	1.60	1.64	1.61	1.65	1.62	1.65
FS_{TWSR_10}	FS_{TWSR_11}	FS_{TWSR_12}	FS_{TWSR_13}	FS_{TWSR_14}	FS_{TWSR_15}	FS_{TWSR_16}	FS_{TWSR_17}
1.73	1.72	1.70	1.69	1.67	1.66	1.65	1.64
FS_{MAXF_1}	FS_{MAXF_2}	FS_{MAXF_3}	FS_{MAXF_4}	FS_{MAXF_5}	FS_{MAXF_6}	FS_{MAXF_7}	FS_{MAXF_8}
1.76	1.78	1.77	1.79	1.78	1.80	1.78	1.81
FS_{MAXF_10}	FS_{MAXF_11}	FS_{MAXF_12}	FS_{MAXF_13}	FS_{MAXF_14}	FS_{MAXF_15}	FS_{MAXF_16}	FS_{MAXF_17}
1.88	1.86	1.84	1.82	1.80	1.79	1.77	1.75
Maximum deflection (δ_{MAX})	LAY9_S_{XMAX}	LAY9_S_{XMIN}	LAY9_S_{YMAX}	LAY9_S_{YMIN}	D_{max}	D_{min}	t_1
0.00218 (m)	158772(Pa)	-28654 (Pa)	219556.6 (Pa)	-69869 (Pa)	2.0838(m)	1.8842(m)	1.59(mm)
Buckling strength factor (λ)	L_{pmb}(m)	T_{cor} (m)	α	Operating depth ($H(m)$)	LAY9_von Mises (Pa)	Drag Force (N)	B.F
118	2.80	0.091	55°	255.00	1636834.95	2.19925×10^{12}	0.47
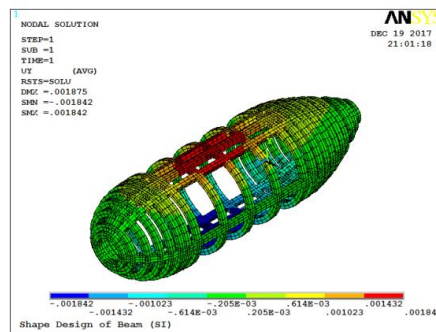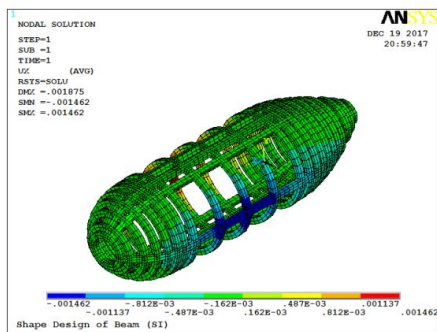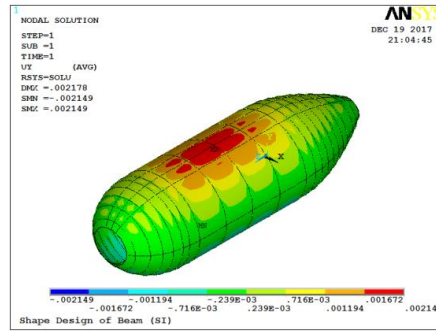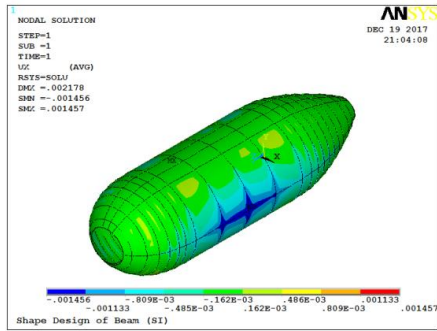
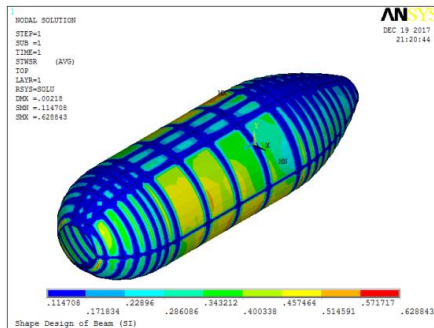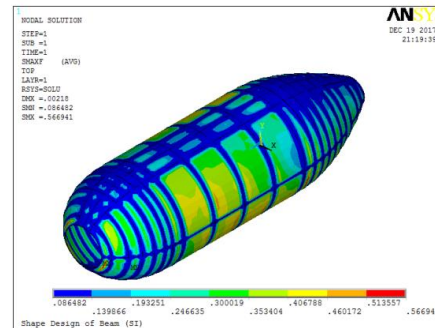a)   Displacement distribution (Ux)   b)   Displacement distribution (Uy)
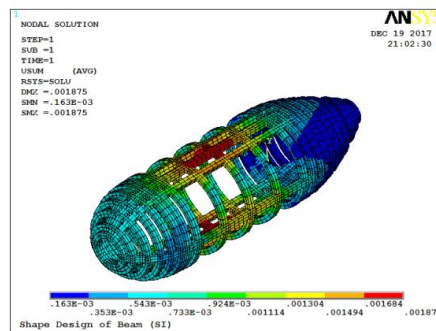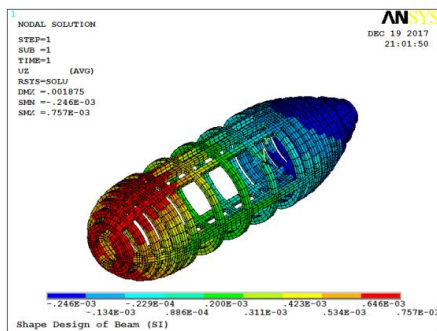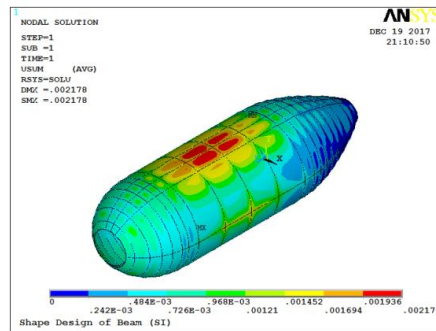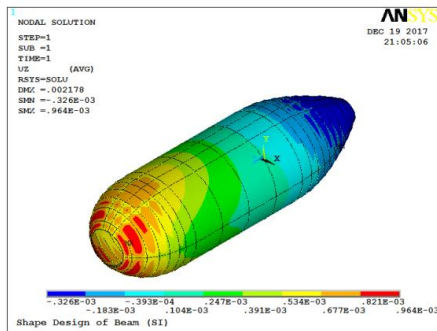
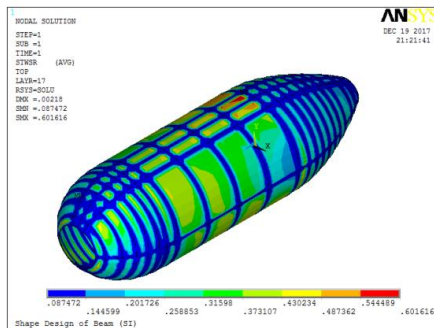c)   Displacement distribution (Uz)   d)   Displacement distribution (U$_{magnitude}$)

Fig. 6 Displacement distribution (Ux,Uy, Uz and U$_{magnitude}$) in composite pressure hull.
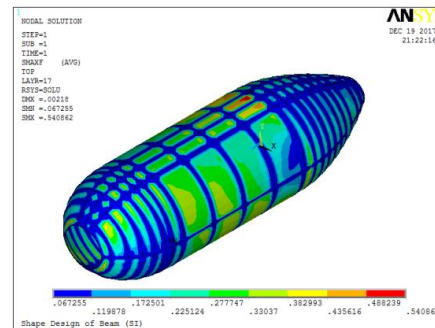
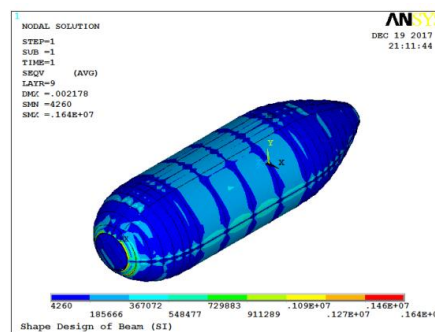a)   Tsai-Wu failure distribution at Ply-1

b)   Maximum stress failure distribution at Ply-1

c)   Tsai-Wu failure distribution at Ply-17

d)   Maximum stress failure distribution at Ply-17

e)   von Mises stress distribution at core layer (Ply-9)

Fig. 7 Tsai-Wu, maximum stress and von Mises distribution in composite pressure hull.

Also, **Table 2** illustrated that, material failure incorporating both Tsai-Wu and maximum stress failure criteria were considered together for predicting the first-ply failure. The minimum factor of safety (FS$_{TWSR}$ and FS$_{MAXF}$) are occurring in the lower face at ply-1 due to maximum tensile stresses and equal 1.59 and 1.76, respectively. At upper face, the minimum values of F_{TWSR} and F_{MAXF} are occurring at ply-17 due to maximum compressive stresses with value equal to 1.64 and 1.75, respectively. The optimized orientation fiber α equals to (55°) with T_{core} of about 91

mm. **Fig. 7** (a, b, c and d) shows the Tsai-Wu and maximum stress failure distribution at critical Plies (Ply-1 and pl-17). The maximum Tsai-Wu and maximum stress failure at ply-1 will be initiates first at the middle of the left and right sides of the composite pressure hull. For ply-17, the failure will be initiates first at the upper and lower regions of the composite pressure hull. **Fig. 7** -e shows the von Mises stress distribution for core layer (Ply-9) and illustrated clearly that, the maximum von Mises stresses occurs at the regions between long and ring beams.

4.1 Effect of fiber orientation on design variables and design constraints

Fig. 8-(a and b) shows the effect of (α) on maximum deflection value (δ_{MAX}) and buckling strength factor (λ). It can be seen that, (δ_{MAX}) equals to 4.63 mm and occurs when α equals to 0°. As (α) increases the maximum deflection value decreases and reaches to the minimum value when α equals to 90° with value equals to 2.04 mm. **Fig. 8**-b shows the variations of buckling strength factor with fiber orientation α. It illustrates that, the minimum buckling strength factor value is equal to 16.5 and occurs when α equals to 0°. After that, as (α) increases (λ) increases and reaches to maximum value when α equals to 60° with value equals to 157.2. With increasing α, (λ) decreases again and reaches to 45 at α equals to 90°.
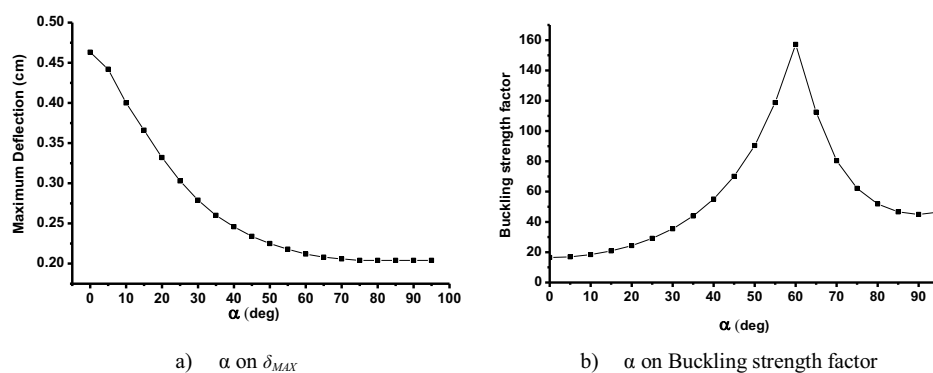
a) α on δ_{MAX} b) α on Buckling strength factor

Fig. 8 The effect of fiber orientation (α) on the buckling strength factor and maximum deflection value (δ_{MAX}).

a)   α on Tsai-Wu failure index (lower face)   b)   α on Tsai-Wu failure index (upper face)

c)   α on maximum stress index (lower face)   d)   α on maximum stress index (upper face)
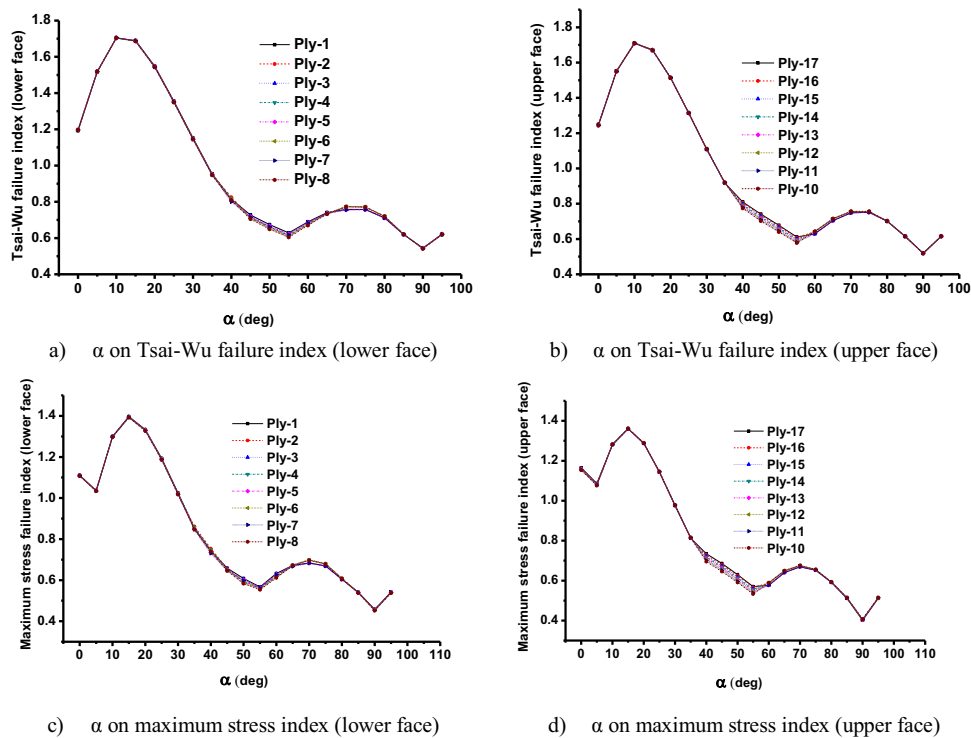
Fig. 9 The effect of fiber orientation (α) on the Tsai-Wu and maximum stress failure index.

Fig. 9 presents the effect of (α) on Tsai-Wu and maximum stress failure index for both upper and lower faces of the sandwich composite pressure hull. The maximum failure indices for Tsai-Wu and maximum stress failures occur when α equals to 10° at lower face with values equal to 1.7 and 1.29, respectively and the maximum occurs at (Ply-1) due to the high tensile stresses. With increasing α, the maximum failure indices for Tsai-Wu and maximum stress decrease and reach to the minimum values when α equals to 55°. After that, the maximum failure indices increase until α equals to 70° with values equal to 0.76 and 0.69 for Tsai-Wu and maximum stress failures, respectively. The maximum failure indices for the lower face decrease until α equals to 90° and reach to the minimum with values equal to 0.55 and 0.52 for Tsai-Wu and maximum stress failures, respectively. For the upper face, the minimum values of Tsai-Wu and maximum stress failure are equal to 0.52 and 0.5, respectively.
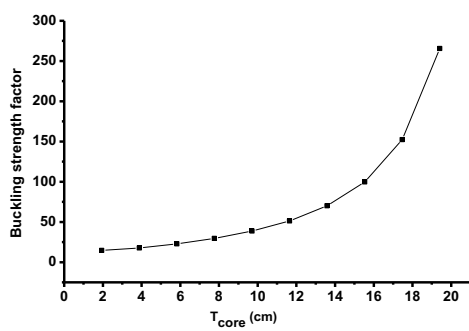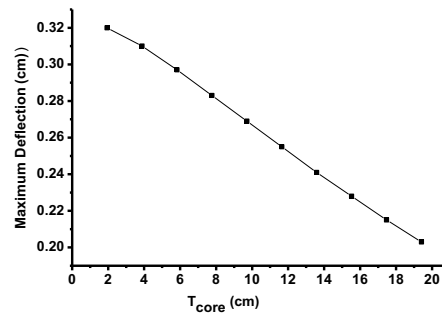
a) T_{core} on Buckling strength factor

b) T_{core} on δ_{MAX}

Fig. 10 The effect of core thickness (T_{core}) on the buckling strength factor and maximum deflection value (δ_{MAX}).
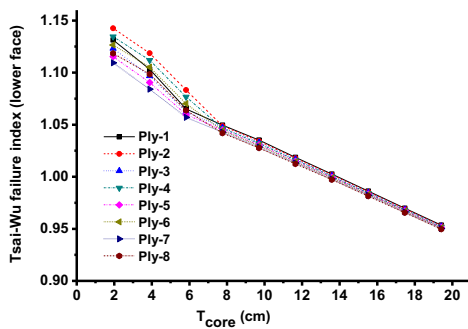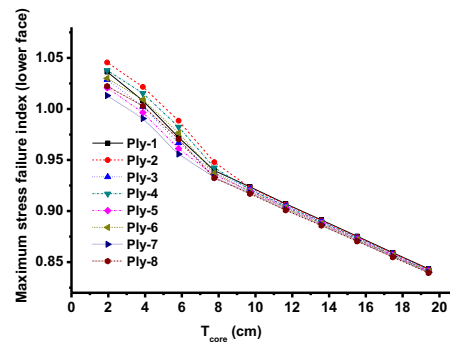

a) T_{core} on Tsai-Wu failure index (lower face)

b) T_{core} on maximum stress failure index (lower face)
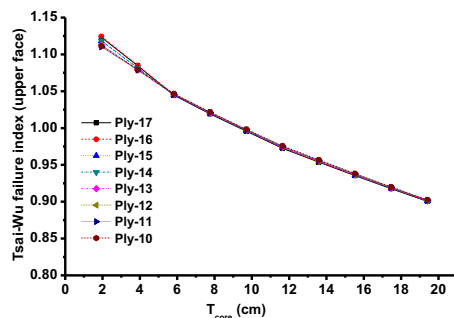
c) T_{core} on Tsai-Wu failure index (upper face)

d) T_{core} on maximum stress failure index (upper face)

Fig. 11 The effect of core thickness (T_{core}) on Tsai-Wu and maximum stress failure index.

4.2 Effect of core thickness (T_{core}) on design variables and design constraints

Fig. 10 illustrates the effect of core thickness (T_{core}) on buckling strength factor and maximum deflection value (δ_{MAX}). The figure shows that, as T_{core}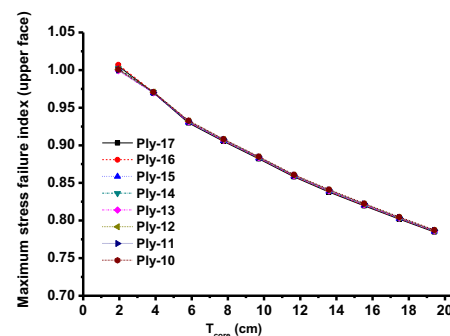 increases the buckling strength factor increases and δ_{MAX} decreases. The results emphasize that, T_{core} has great effect on buckling strength factor. **Fig. 11** presents the effect of T_{core} on maximum Tsai-Wu and maximum stress

failure indices. It reveals that, increasing T_{core}, decreasing the failure index and the core thickness has moderate effect on both Tsai-Wu and maximum stress failure index.

a) L_{pmb} on Tsai-Wu failure index ((lower face)   *b)* L_{pmb} on Tsai-Wu failure index (upper face)

c) L_{pmb} on maximum stress failure index (lower face)   *d)* L_{pmb} on maximum stress failure index (upper face)
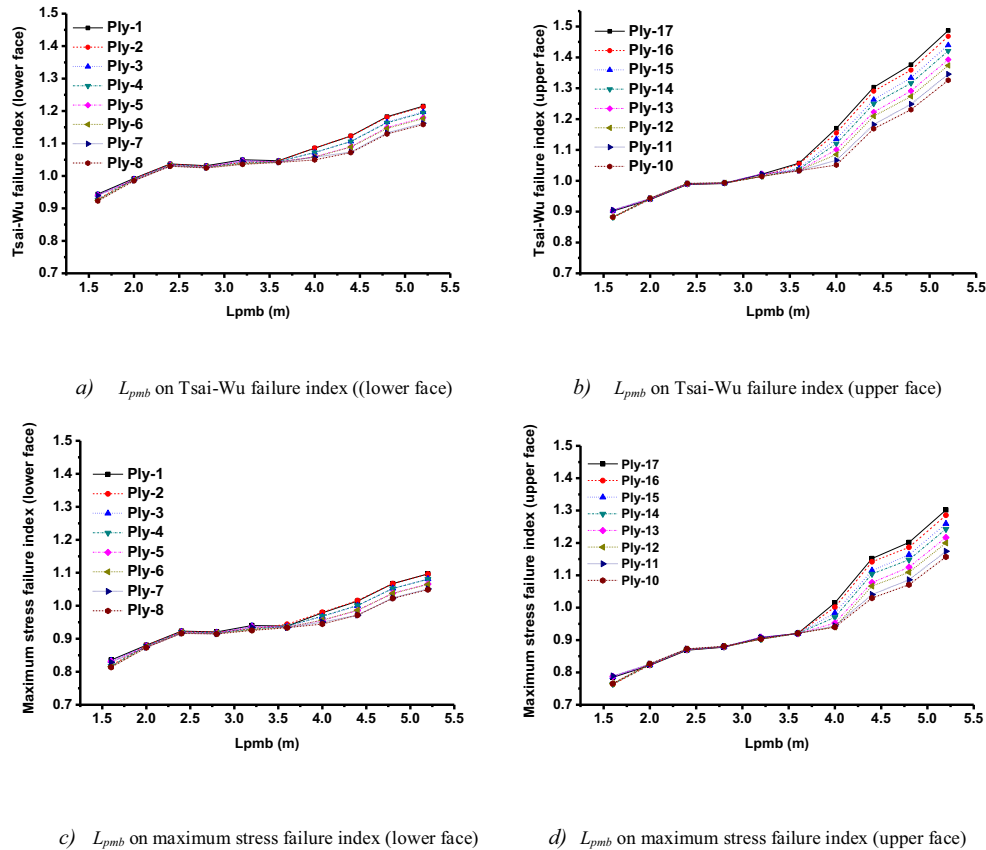
Fig. 12 Effect of (L_{pmb}) on Tsai-Wu and maximum stress failure index.

5. Conclusions

In this study the finite element simulation and optimization were presented for increasing the buckling load capacity, minimizing the drag force and the weight/displacement ratio using ANSYS (APDL). The following observations were made:

- The pattern of optimum points is presented which is used in fabricating and designing the composite pressure hull under hydrostatic pressures.

- At lower face sheet the failure will be initiate first at (ply-1), for upper face sheet the failure will be initiate at the upper most layer (ply-17).

- The core thickness is important to resist the shell buckling.

- The fiber orientation angle (α) has a great effect on buckling strength factor, maximum deflection value, Tsai-Wu and maximum stress failure index of the sandwich composite pressure hull.

- The results suggest that, in the design of composite pressure hull, both buckling and material failure should be considered.

References

[1] Helal M, Huang H, Wang D, Fathallah E. Numerical Analysis of Sandwich Composite Deep Submarine Pressure Hull Considering Failure Criteria. Journal of Marine Science and Engineering. 2019;7(10):377.

[2] Fathallah E, Qi H, Tong L, Helal M. Multi-Objective Optimization of Composite Elliptical Submersible Pressure Hull for Minimize the Buoyancy Factor and Maximize Buckling Load Capacity. Applied Mechanics and Materials. 2014;578:75-82.

[3] Zhang J, Zhang M, Tang W, Wang W, Wang M. Buckling of spherical shells subjected to external pressure: A comparison of experimental and theoretical data. Thin-Walled Structures. 2017;111(Supplement C):58-64.

[4] Zhang M, Tang W, Wang F, Zhang J, Cui W, Chen Y. Buckling of bi-segment spherical shells under hydrostatic external pressure. Thin-Walled Structures. 2017;120(Supplement C):1-8.

[5] Pranesh SB, Kumar D, Subramanian VA, Sathianarayanan D, Ramadass GA. Non-linear buckling analysis of imperfect thin spherical pressure hull for manned submersible. Journal of Ocean Engineering and Science. 2017.

[6] Zhang J, Zhang M, Cui W, Tang W, Wang F, Pan B. Elastic-plastic buckling of deep sea spherical pressure hulls. Marine Structures. 2018;57(Supplement C):38-51.

[7] Topal U, Uzman U. Multiobjective Optimization of Angle-ply Laminated Plates for Maximum Buckling Load. Finite Elementsin Analysis and Design. 2010;46(3):273-9.

[8] Błachut J, Smith P. Buckling of multi-segment underwater pressure hull. Ocean Engineering. 2008;35(2):247-60.

[9] Carvelli V, Panzeri N, Poggi C. Buckling strength of GFRP under-water vehicles. Composites Part B: Engineering. 2001;32(2):89-101.

[10] Błachut J. Buckling of composite domes with localised imperfections and subjected to external pressure. Composite Structures. 2016;153(Supplement C):746-54.

[11] Fathallah E, Qi H, Tong L, Helal M. Optimal Design Analysis of Composite Submersible Pressure Hull. Applied Mechanics and Materials. 2014;578:89-96.

[12] Fathallah E, Qi H, Tong L, Helal M. Design Optimization of Composite Elliptical Deep-Submersible Pressure Hull for Minimizing the Buoyancy Factor. Advances in Mechanical Engineering. 2014.

[13] Fathallah E. Finite Element Modelling and Multi-Objective Optimization of Composite Submarine Pressure Hull Subjected to Hydrostatic Pressure. Materials Science Forum. 2019;953: 53-8.

[14] Helal M, Fathallah E. Multi-objective optimization of an intersecting elliptical pressure hull as a means of buckling pressure maximizing and weight minimization. Materials Testing. 2019;61(12):1179-91.

[15] Helal M, Huang H, Fathallah E, Wang D, ElShafey MM, Ali MAEM. Numerical Analysis and Dynamic Response of Optimized Composite Cross Elliptical Pressure Hull Subject to Non-Contact Underwater Blast Loading. Applied Sciences. 2019;9(17):3489.

[16] Fathallah E, Helal M. Optimum Structural Design of Deep Submarine Pressure hull to achieve Minimum

Weight. The International Conference on Civil and Architecture Engineering. 2016;11(11PthP International Conference on Civil and Architecture Engineering):1-22.

[17] Alogla A, Helal M, Abdal Allah AA, Fathallah E. Design Optimization of a Flexible Hinge Compliant Micro icro-Gripper ripper Mechanism with Parallel Movement Arms Using Pseudo-Rigid -Body Model. International Conference on Aerospace Sciences and Aviation Technology. 2017;17(AEROSPACE SCIENCES & AVIATION TECHNOLOGY, ASAT - 17 – April 11 - 13, 2017):1-18.

[18] Zhang J, Wang M, Wang W, Tang W, Zhu Y. Investigation on egg-shaped pressure hulls. Marine Structures. 2017;52(Supplement C):50-66.

[19] Vosoughi AR, Darabi A, Dehghani Forkhorji H. Optimum stacking sequences of thick laminated composite plates for maximizing buckling load using FE-GAs-PSO. Composite Structures. 2017;159(Supplement C):361-7.

[20] Mian HH, Wang G, Dar UA, Zhang W. Optimization of Composite Material System and Lay-up to Achieve Minimum Weight Pressure Vessel. Applied Composite Materials. 2013;20:873–89.

[21] Pan G, Lu J, Shen K, Ke J. Optimization of Composite Cylindrical Shell Subjected to Hydrostatic Pressure. Springer International Publishing Switzerland 2015:81-90.

[22] Fathallah E, Helal M. Finite element modelling and multi-objective optimization of composite submarine pressure hull subjected to hydrostatic pressure. IOP Conference Series: Materials Science and Engineering. 2019;683:012072.

[23] Imran M, Shi D, Tong L, Waqas HM. Design optimization of composite submerged cylindrical pressure hull using genetic algorithm and finite element analysis. Ocean Engineering. 2019;190:106443.

[24] Lund E. Discrete Material and Thickness Optimization of laminated composite structures including failure criteria. Structural and Multidisciplinary Optimization. 2018;57(6):2357-75.

[25] Fathallah E, Qi H, Tong L, Helal M. Design optimization of lay-up and composite material system to achieve minimum buoyancy factor for composite elliptical submersible pressure hull. Composite Structures. 2015;121(Supplement C):16-26.

[26] Vinson JR, L R. The Behavior Of Structures Composed Of Composite Materials: Springer, Dordrecht; 2008.

[27] Kaw AK. Mechanics of Composite Materials. Second Edition ed: CRC Press Taylor & Francis Group; 2006.

[28] Soden PD, Hinton MJ, Kaddour AS. A comparison of the predictive capabilities of current failure theories for composite laminates. Composites Science and Technology. 1998;58(7):1225-54.

[29] Paster D, Co R, Portsmouth, RI. Importance of Hydrodynamic Considerations for Underwater Vehicle Design. In: Proceedings of MTS/IEEE Oceans. Washington, DC, USA, Conference, Conference 23-25 Sept. 1986. p. 1413-22.

[30] Alam K, Ray T, Anavatti SG. Design of a Toy Submarine Using Underwater Vehicle Design Optimization Framework. IEEE. 2011.

[31] M.A.Martz. Preliminary design of an autonomous underwater vehicle using a multiple-objective genetic optimizer [Master'sthesis]. Blacksburg,VA,United States: Virginia Polytechnic Institute and State University; 2008.

[32] Alam K, Ray T, Anavatti SG. Design and construction of an autonomous underwater vehicle. Neurocomputing. 2014;142(Supplement C):16-29.

[33] Alvarez A, Bertram V, Gualdesi L. Hull hydrodynamic optimization of autonomous underwater vehicles operating at snorkeling depth. Ocean Engineering. 2009;36(1):105-12.

[34] Zheng JY, Liu PF. Elasto-plastic Stress Analysis and Burst Strength Evaluation of Al-carbon Fiber/Epoxy Composite Cylindrical Laminates. Computational Materials Science. 2008;42(3):453-61.

[35] Panahi B, Ghavanloo E, Daneshmand F. Transient Response of a Submerged Cylindrical Foam Core Sandwich Panel Subjected to Shock Loading. Materials & Design. 2011;32(5):2611-20.

[36] Smith CS. Design of submersible pressure hulls in composite materials. Marine structures. 1991;4:141-82.

[37] Inc A. ANSYS Theory Reference Release 14.5. October ed2012.

[38] M. Erdogan GI. The Finite Element Method and Applications in Engineering Using ANSYS. New York: Springer; 2006.

[39] Liang CC, Chen HW, Jen CY. Optimum Design of Filament-wound Multilayer Sandwich Submersible Pressure Hulls. Ocean Engineering. 2003;30(15):1941-67.

[40] Ross CTF. A conceptual Design of an Underwater Vehicle. Ocean Engineering. 2006;33(16):2087-104.

[41] Ma S, Mahfuz H. Finite Element Simulation of Composite Ship Structures with Fluid Structure Interaction. Ocean Engineering. 2012;52:52-9.